journal

J Am Ceram Soc, 95 [2] 538–544 (2012)
DOI: 10.1111/j.1551-2916.2011.04920.x

Thickness-Dependent Dielectric, Ferroelectric, and Magnetodielectric Properties of $BiFeO_3$ Thin Films Derived by Chemical Solution Deposition

Xianwu Tang,[‡,†] Jianming Dai,[‡] Xuebin Zhu,[‡,†] Jianchao Lin,[‡] Qing Chang,[‡] Dajun Wu,[‡] Wenhai Song,[‡] and Yuping Sun[‡,§]

[‡]Key Laboratory of Materials Physics, Institute of Solid State Physics, Chinese Academy of Sciences, Hefei 230031, China

[§]High Magnetic Field Laboratory, Chinese Academy of Sciences, Hefei 230031, China

Thickness is a very important parameter to control the microstructures, as well as physical properties in the multiferroic $BiFeO_3$ thin films. In this article, $BiFeO_3$ thin films with different thickness (from 210 to 830 nm) are fabricated by chemical solution deposition on the $Pt/Ti/SiO_2/Si$ (100) substrates to investigate the thickness effects systematically. The results show that the crystallization is improved, the dielectric constant is enhanced, and the leakage current is reduced with increasing thickness. On the other hand, the magnetization and magnetodielectric are decreased with thickness. The results show that the optimized thickness should be within the range of 400–600 nm to obtain optimized properties using chemical solution deposition processing, which will provide a useful guidance to prepare the multiferroic $BiFeO_3$ thin films.

I. Introduction

Multiferroics can be used as actuators, switches, magnetic field sensors, and new types of electronic memory.[1,2] The $BiFeO_3$ (BFO), as the room temperature multiferroic single-phase material, has an important value of applications, as well as investigation in understanding its physical properties.[3–5] However, it is realized that it is difficult to apply the BFO ceramics into applications due to the large leakage current from its low resistivity characteristics.[1] One plausible way to solve such problem is to prepare BFO thin films. To date, various methods, including magnetron sputtering,[6] pulsed laser deposition,[1] and metal organic chemical vapor deposition[7] have been used to prepare BFO thin films, as well as to optimize the properties. Chemical solution deposition (CSD) as an alternative route and widely used to fabricate lots of functional thin films due to its advantages[8] has been also used to prepare BFO films.[9–11]

To avoid large leakage current and to obtain good room-temperature ferroelectric properties, the thickness of BFO thin films should be larger than a certain value. The value is about 250 nm for the physical-derived BFO thin films[1,2,6] and 400 nm for the CSD-derived one.[10,11] Meanwhile, the BFO thin films show improved ferroelectric properties with increase in the films' thickness.[6,11] Hence, it is to deduce that the thick bulk disks should have better polarization characteristics than the properties of thin films, while it is contrary to the facts. Thus, the thickness effects should be a balanced result by competitive effects and deserve investigating systematically.

In this article, BFO thin films with thickness from 210 to 830 nm are prepared, and the thickness effects on the microstructure, dielectric, ferroelectric, magnetic, and magnetodielectric properties have been investigated systematically.

II. Experimental Procedure

The CSD-derived BFO thin films studied in this work are fabricated on $Pt/Ti/SiO_2/Si$ (100) substrate with 0.2 *M* precursor solution, and pyrolysis each coating layer at 350°C for 10 min in air, which is same as in our previous works.[12] To increase the thickness, the spinning coating and pyrolysis processes are repeated for 10, 15, 20, 30, 40 times, respectively. Finally, the deposited films are annealed at 550°C for 10 min in nitrogen. The corresponding films, for the sake of simplify describing, are defined as T10, T15, T20, T30, and T40, respectively.

X-ray diffraction (XRD) using a Philips X'pert Pro diffractormeter with CuK_α radiation is used to check up crystallization quality and out-of-plane orientation of the derived thin films. Field-emission scanning electron microscopy (FE-SEM; FEI Sirion 200 type, FEI, Hillsboro, OR) is used to detect the thickness and surface morphology. Magnetic properties of the films are measured using Quantum Design vibrating-simple magnetometer (VSM) (PPMS-9). Top Au electrodes of 0.2 mm diameter are deposited by sputtering with Miriam small ion sputtering (SCB-12) on the surface of BFO layer through a shadow mask. The films' room-temperature dielectric response is investigated within 100 Hz–1 MHz frequency range with a driving voltage 1 V using precision LCR meter model TH2828/A/S. The ferroelectric and leakage properties are investigated using a Sawyer–Tower circuit attached to a computer-controlled standardized ferroelectric test system (Precision Premier II; Radiant Technologies, Albuquerque, NM). Magnetodielectric is determined by measuring the variation of dielectric responses with magnetic fields produced by the Quantum Design superconducting quantum interference device at 300 K with a frequency of 100 kHz.

III. Results and Discussions

(1) Microstructure

Figure 1 shows the XRD patterns of the BFO films with different thicknesses. All the films are randomly oriented without parasitic phases. All peaks can be indexed to a perovskite structure with pseudocubic unit cell. As the strain is an important role on the ferroelectric properties of the films,[13] the lattice constant a of the derived films is calculated and the strain is defined as ($\varepsilon = (a - a_0)/a_0 \times 100\%$) where a_0 is taken as 3.97 Å.[14] The inset (a) of the Fig. 1 is the lattice constant and ε versus thickness result. It is observed that the lattice constant and the compression strain are increased and decreased with thickness, respectively. The above-mentioned tendency can be attributed to the stress relaxation induced by the difference of

X. Tan—contributing editor

Manuscript No. 29844. Received June 09, 2011; approved September 27, 2011.
[†]Authors to whom correspondence should be addressed. e-mails: xwtang@issp.ac.cn and xbzhu@issp.ac.cn

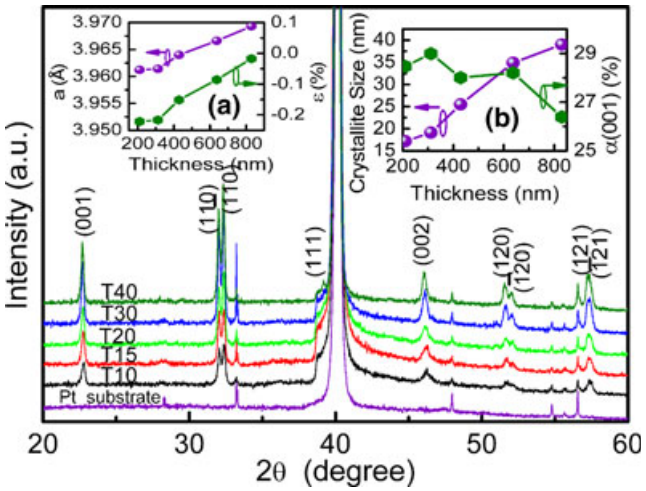

Fig. 1. X-ray diffraction for the CSD-derived BFO thin films prepared on the $Pt/Ti/SiO_2/Si$ (100) substrate with different thickness. Variation of lattice constant and strain with the films' thickness are shown in the inset (a). The crystallite and (001)-orientation with changing films thickness are shown in the inset (b).

thermal expansion coefficient between BFO (6×10^{-5}/°C) and the substrate Pt (8.9×10^{-6}/°C).[15]

As the orientation of thin films will apply obvious effects on the microstructure and properties,[12,16] it is desirable to estimate the texture. The (001)-orientation degree is defined as $\alpha(001) = I_{001}/(I_{001} + I_{110} + I_{\bar{1}10}) \times 100\%$ where I_{001}, I_{110}, and $I_{\bar{1}10}$ is the intensity of the BFO (001), (110), and ($\bar{1}$10) peak diffraction pattern, respectively.[17] The α(001) value and crystallite size calculated with Scherrer's formula[18] versus the films' thickness are plotted in the inset (b) of Fig. 1. It can be seen that the crystallite size increases with thickness, and all the crystallite size is smaller than 62 nm (the BFO spiral spin modulation wave length[3]). The increased BFO crystallite size can be attributed to the successive pyrolysis steps during the preparing process. Similar to our previous reports,[12] the value of the α(001) increases with decreasing thickness, which originates from the depression of bulk homogenous nucleation.[12]

Figure 2 shows the cross-section FE-SEM results of all the BFO films. The thickness detected from the figure for the films T10, T15, T20, T30, and T40 is 210, 312, 429, 637, and 830 nm, respectively. Furthermore, it indicates a thickness of 20 nm for each coating/pyrolysis layer. The FE-SEM results for the surface morphology of all thin films are shown in Fig. 3. It is observed that the average BFO grain size

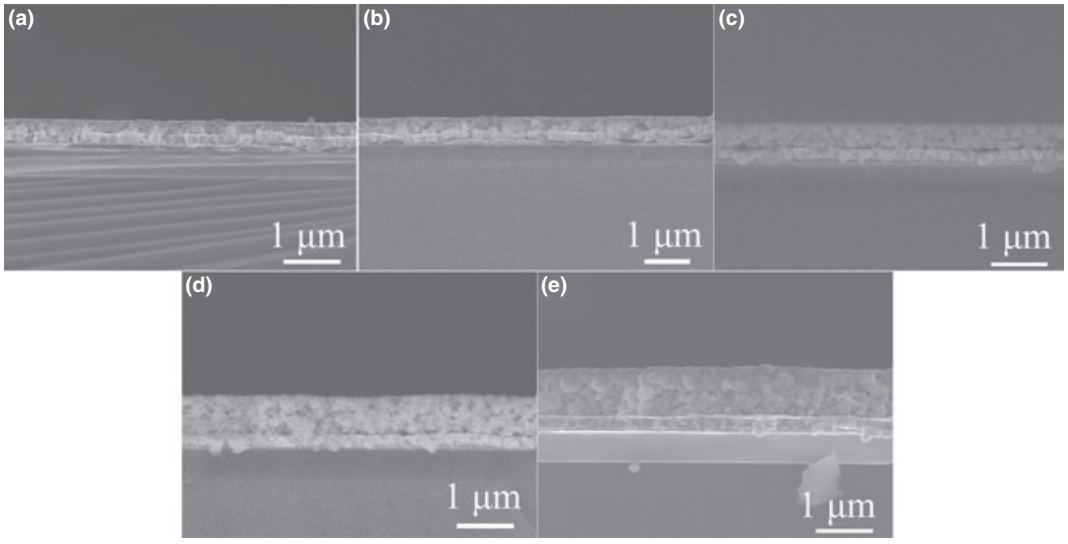

Fig. 2. The cross-section of FE-SEM results for the BFO thin films (a) T10, (b) T15, (c) T20, (d) T30, and (e) T40.

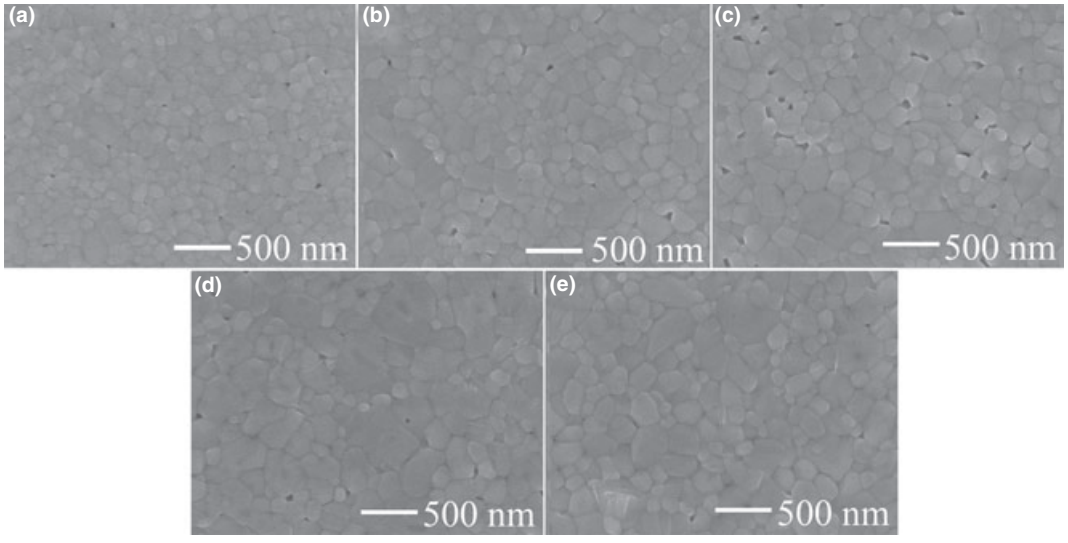

Fig. 3. The FE-SEM results for the surface morphology of the BFO thin films (a) T10, (b) T15, (c) T20, (d) T30, and (e) T40.

increases with thickness, which is same as that of crystallite sizes shown in Fig. 1(c). The increase in average grain size may be caused by the higher thermal budget.[19] Moreover, when the thickness is larger than 600 nm, a number of microcracks can be observed and can be caused by residual stress created due to the mismatch of thermal expansion coefficients.[8,20]

(2) Dielectric Properties

The frequency dependence of relative dielectric constant (ε_r) and dielectric loss (tan δ) for all thin films is displayed in the Figs. 4(a) and (b), respectively. It can be found that the dielectric constant increases and the dielectric loss decreases with thickness within the measured frequency ranges (the magnified dielectric losses of all the films in the low frequency are not shown here). To give a clear image, variation of dielectric constant and loss measured at 1 MHz with the films' thickness are plotted in the inset of the Fig. 4(b). It is clearly seen that the value of ε_r increases from 135 to 181 and the tan δ decreases from 0.28 to 0.05 when the films' thickness increases from 210 to 830 nm, respectively.

It is well-known that the dielectric permittivity of the ferroelectric thin films consists of intrinsic and extrinsic contributions.[19,21] Among the intrinsic factors, the dielectric response

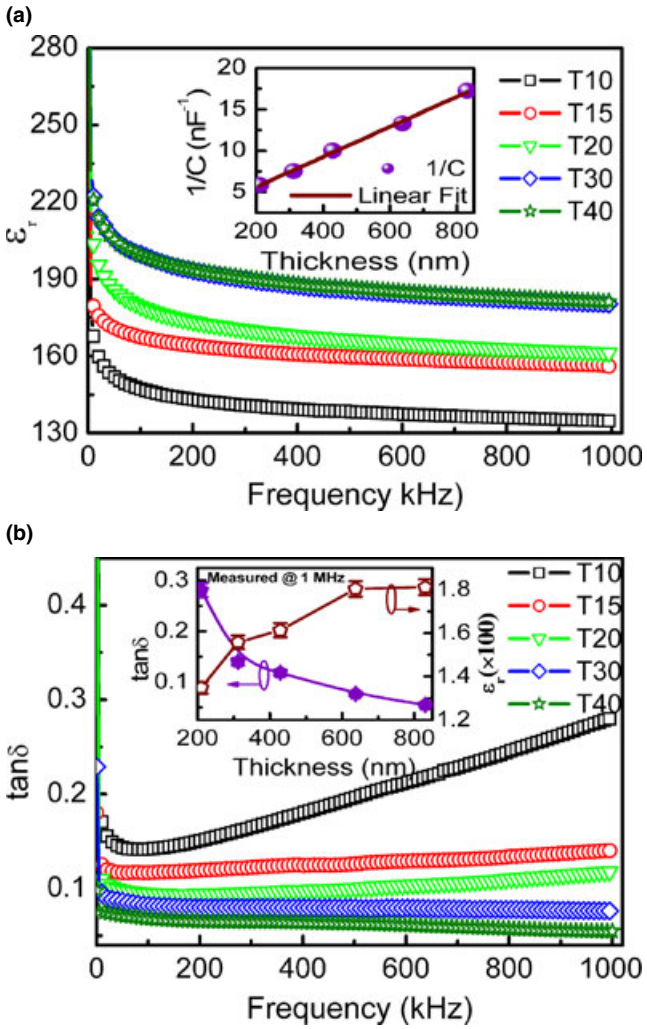

Fig. 4. (a) Room temperature frequency dependence of dielectric constant (ε_r) of all the films. The reciprocal capacitance measured at 1 MHz versus films' thickness and a linear fitting are shown in the inset. (b) Room temperature frequency dependence of dissipation factor, tan δ on the thickness of BFO films. The inset shows the dependence of tan δ and ε_r measured at 1 MHz versus films' thickness.

of the single domains,[21] films orientation, and grain size are the more important ones.[19] The (001)-oriented BFO has the largest relative dielectric permittivity.[16] However, in our films, the BFO thin films with lower (001)-orientation have the higher relative dielectric permittivity. It indicates that the orientation plays a subtle role in determination of dielectric constant. While the decrease in grain size can lead an increase in the internal stresses to inhibit the forming 180° domains and decrease the electric constant followed in some ferroelectric films.[19] Thus, the increase in grain size in our films maybe also favors forming 180° domains and increasing the dielectric constant further, as the films' thickness increases.

The extrinsic contributions are mainly composed of two elements.[19,21] One is that affects the dielectric response of the domain wall motions, such as the mechanical strain/stress from the substrate clamping and pinning of grain boundary. Both the strain from the substrate clamping suggested by the inset (a) of Fig. 1 and the numbers of the grain boundaries shown in Fig. 3 decrease with increase in the films' thickness, which will increase the dielectric constant of the BFO films.

The other is the interfacial layer existed between the films and electrode, which cannot be avoided and is in the series with the capacitance.[22] Moreover, the presence of the interface layer can be inferred by plotting the reciprocal measured capacitance of the BFO films as a function of films' thickness. The reciprocal measured capacitance can be described as $1/C = 1/C_i + (d - t_i)/\varepsilon_f\varepsilon_0 A$ where C_i is the capacitance of the interfacial layer, d is the films' thickness, t_i is the interfacial layer thickness, A is the area of the electrode, ε_f is the BFO films bulk relative permittivity, and ε_0 is the permittivity of vacuum.[19,21] In addition, $1/C = 1/C_i + d/\varepsilon_0\varepsilon_f A$, which assumes that the interfacial layer is negligibly thin compared with the measured BFO films thickness. The reciprocal capacitance as a function of films' thickness measured at 1 MHz and the fitting result are shown in the inset of Fig. 4(a). Based on the fitting results, it is found that there exists an interfacial layer with the value of C_i and ε_f as 0.5 nF and 199.9, respectively. The relative permittivity constant of the interfacial layer calculated further is between 2 and 10, assuming the interfacial layer thickness of 1–5 nm.[19] This means that the interfacial layer with smaller dielectric constant can cause a noticeable decrease in the dielectric constant of the thinner films, while such effect decreases with increasing thickness.

In summary, with increase in the BFO films' thickness, the increase in dielectric constant is attributed to the increase in grain size, decrease in substrate clamping and grain boundary pinning, and the reduced influence of the interfacial layer. Meanwhile, the reduction of grain boundary pinning for the domain wall motion also decreases the dielectric loss of the films as the films' thickness increases.

(3) Leakage Properties

The leakage current density (J) as a function of electric field measured at room temperature for all the BFO thin films are shown in Fig. 5. The leakage current density of each film increases as the electric field is increased. The asymmetric behavior for the positive and negative electric field may be attributed to the asymmetric electrodes in metal–ferroelectric–metal configuration.[9] It is also shown that, the leakage current density decrease from 3.3×10^{-2} to 6.5×10^{-3} A/cm^2 at 200 kV/cm with thickness.

To study the leakage behavior, the space-charge-limited current (SCLC) mechanism is first carried out. The log(J) as a function of log(E) of the films T10, T15, T20, T30, and T40 are plotted in Figs. 6(a)–(e), respectively. A power law relationship log(J) – $s$log(E) is used to fit the curves.[23–26] As a result, all the curves can be well fitted by three straight lines in log–log plots. The fitting value of s_1 in the low field region is around 1 and of s_2 is around 2 in the middle field region, which agrees well with the SCLC mechanism.[23]

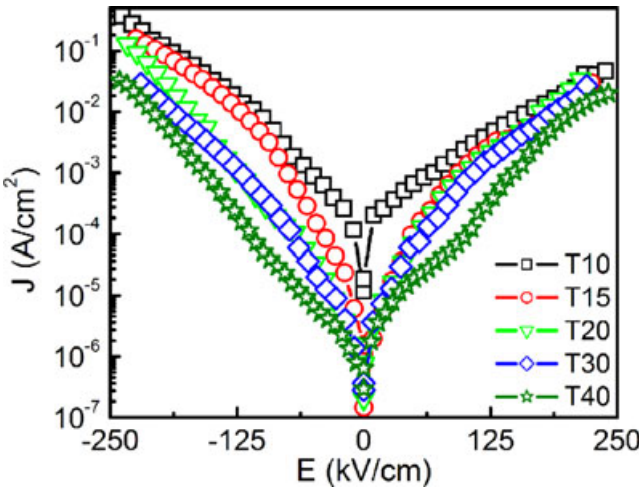

Fig. 5. Room temperature leakage current of the BFO thin films with different thickness.

The space-charge-limited electric field E_{SCL} (Ohmic to modified Child's law) is 59.6, 18.2, 19.8, 24.0, and 24.1 kV/cm for the films T10, T15, T20, T30, and T40, respectively. In higher electric field region, it shows an abrupt increase in the leakage current with the value of s_3 being 3.4, 3.5, 3.7, 3.9, and 5.8 for the T10, T15, T20, T30, and T40, respectively.

The abrupt increase in leakage current maybe originated from all the available traps becoming filled by the applied voltage, and can be well explained by the trap-filled-limit (TFL) law.[24] The electric field at which this abrupt increase occurs is called trap-filled-limit electric field symbolized with E_{TFL}. The E_{TFL} is determined by the law relationship, $E_{TFL} = eN_t d/2\varepsilon_r\varepsilon_0$ where N_t is the total traps density, d is the thickness of the films, ε_r is the films' relative permittivity, and e is the electron charge.[24] The E_{TFL} results with the films' thickness are shown in Fig. 6(f). In addition, combining the measured dielectric constant and films thickness, the value of N_t is calculated and is also plotted in the Fig. 6(f) versus the films' thickness. It is observed that the value of N_t decreases first and then increases with increase in the films' thickness, and exhibits a similar behavior as that of the E_{TFL}. The decrease in N_t and E_{TFL} may result from the reduction in the grain boundaries acted as one of charge trapping centers.[27,28] In addition, it is suggested that the reduction of the concentration of the oxygen vacancies will be also decreased,[5,29,30] although accurate X-ray photoelectron spectroscopic measurements of the films are needed. On the other hand, the cracks, existed in the thicker BFO thin films and acted as the trap centers at the vicinity of the electrodes,[31] will increase the values of N_t and E_{TFL} of the films.

Moreover, the existence of interfacial layer between the electrode and films can also affect the leakage behavior of the BFO thin films. Thus, the Fowler–Nordheim (FN) tunneling mechanism is also used to check the leakage of all the films. From the fitting results shown in Figs. 7(a)–(e), it can be seen that the leakage currents of the films only show FN tunneling behavior above the electric field E_{FN}, where the E_{FN} relates to the potential barrier height of the interfacial layer.[32] To give a clear variation of the E_{FN} with the films' thickness, the value of E_{FN} versus the films thickness is plotted in the Fig. 7(f). The decrease in the value of the E_{FN} with the increasing thickness is observed and suggests that the influence of the interfacial layer on the leakage reduce with increase in the films' thickness. In addition, the leakage current density cannot be fitted well using Poole–Frenkel or Schottky emission conductions mechanism.

Briefly, the conduction mechanisms of the CSD-derived BFO thin films are dominant with Ohmic mechanism in the low electric fields, SCLC mechanism in the middle electric fields, and FN tunneling mechanism in the high electric fields. The contribution of the FN tunneling caused by the interfacial layer to the leakage current decreases with increase in the films' thickness. The reduction in the leakage current of the BFO thin films is a result of combined effects of the change in trapping center and the influence of the interfacial layer.

(4) Ferroelectric Properties

Figure 8 shows the polarization evolution with thickness as a function of the electric field for the derived BFO thin films. As shown in Fig. 8(a), it is difficult to obtain a ferroelectric

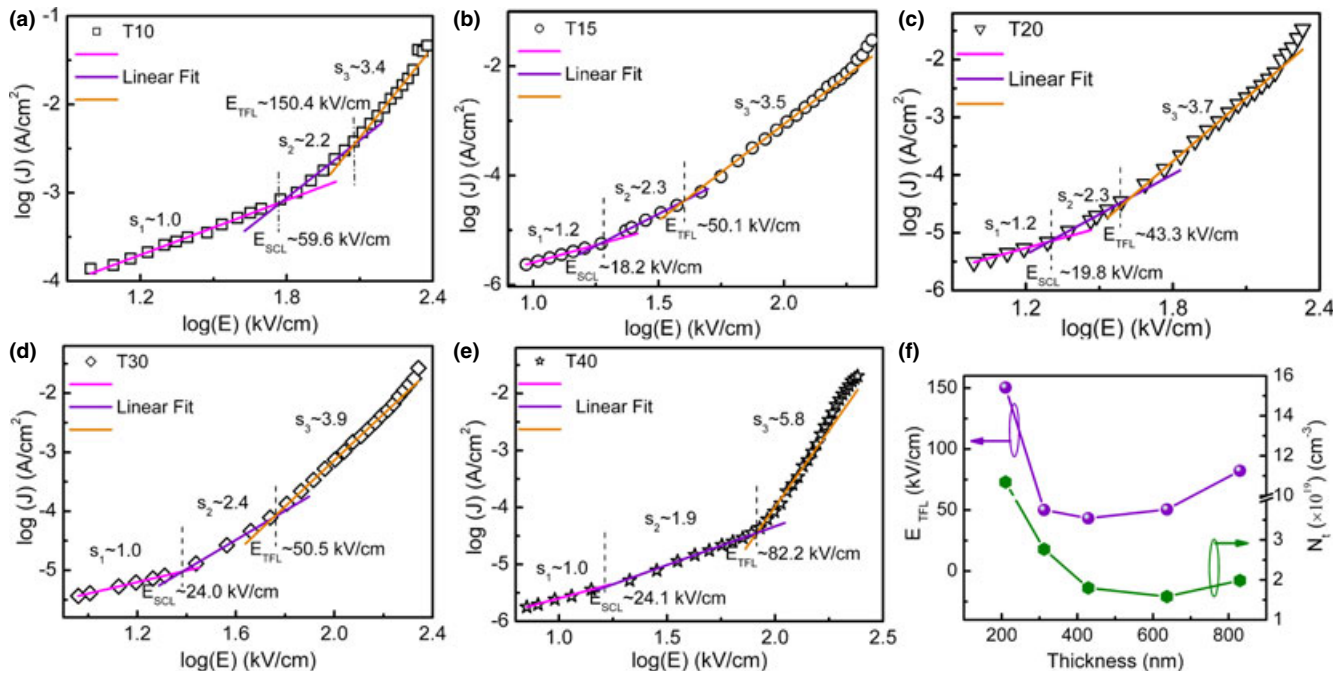

Fig. 6. Leakage current density fitted by space-charge-limited conduction mechanism for the BFO thin films (a) T10, (b) T15, (c) T20, (d) T30, and (e) T40. The dependence of the values of trap density N_t and trap-filled-limit electric field E_{TFL} on the films' thickness are plotted in (f).

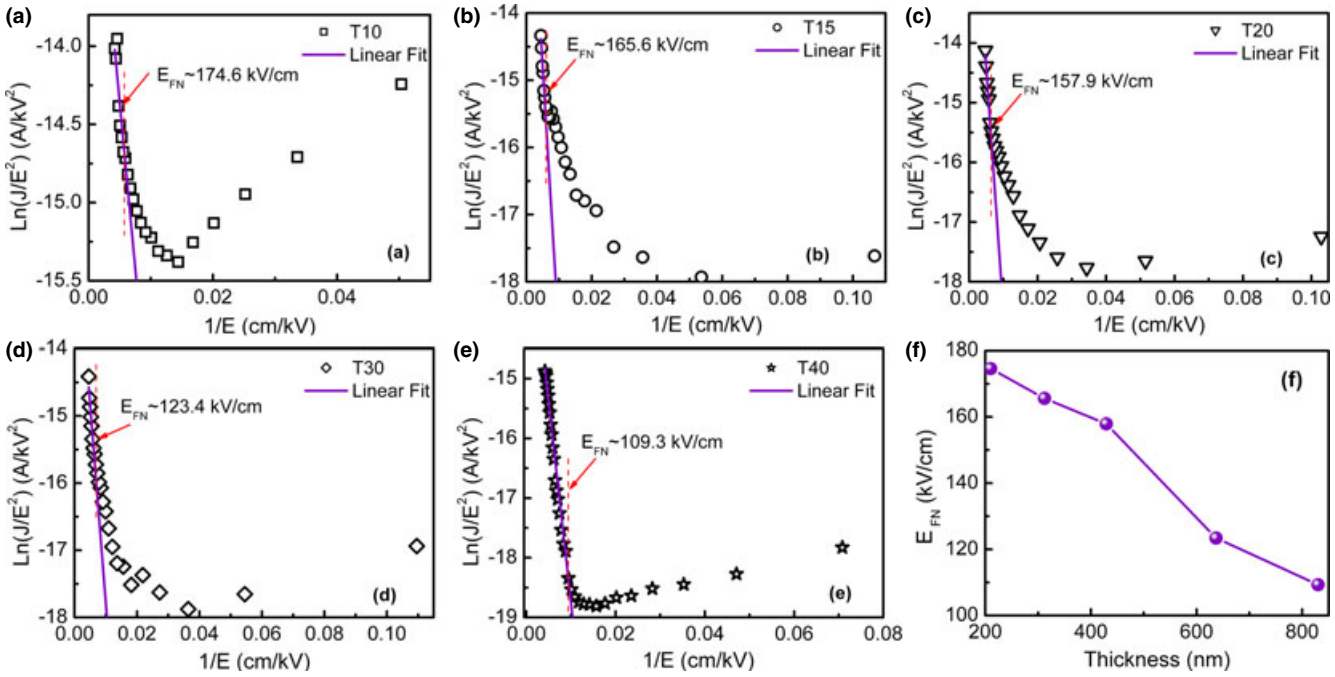

Fig. 7. Leakage current density fitted by Fowler–Nordheim tunneling conduction mechanism for the BFO thin films (a) T10, (b) T15, (c) T20, (d) T30, and (e) T40. The value of E_{FN} dependence of the films' thickness is plotted in (f).

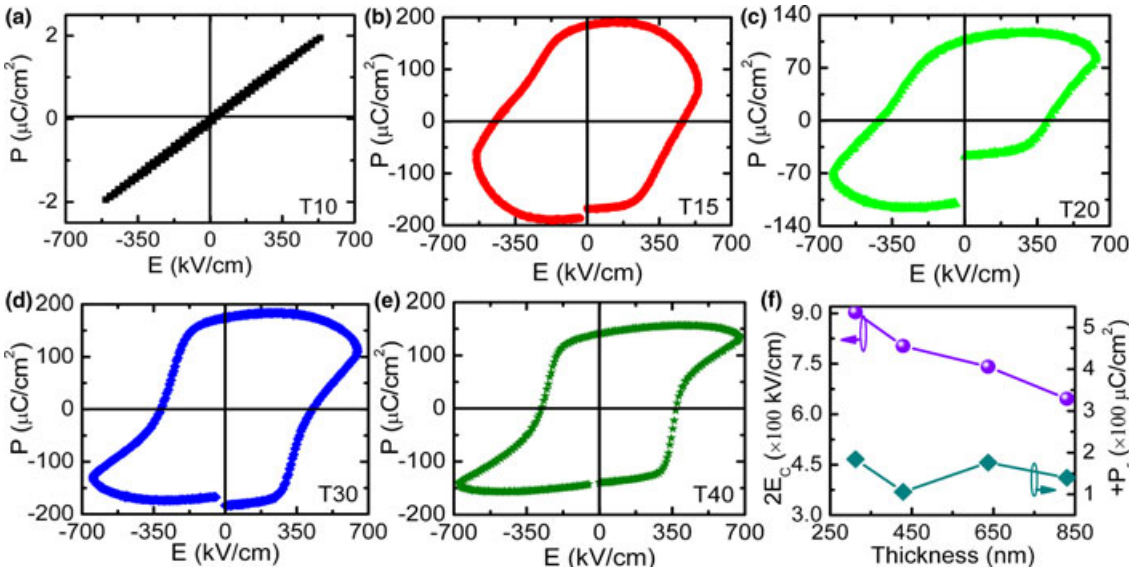

Fig. 8. Ferroelectric hysteresis loops measured at room temperature with 20 kHz frequency of samples of (a) T10, (b) T15, (c) T20, (d) T30, and (e) T40. (f) The thickness dependence of the positive remnant polarization ($+P_r$) and the coercive field ($2E_c$).

hysteresis loop for the 210 nm thick BFO film (T10) due to serious leakage current. The saturated ferroelectric hysteresis loop can be obtained with the increasing thickness. To give a clear image of the films' thickness effect on the ferroelectric properties, Fig. 8(f) displays the variation of the positive remnant polarization ($+P_r$) (here, just defined as the polarization at the zero electric filed) and the coercive field ($2E_c$) (defined as the electric filed at the zero polarization) with different thickness, except for the sample T10.

As shown in the Fig. 8(f), the thickness effect on the remnant polarization is very weak. As the contribution of leakage current cannot be avoided in the measurements of ferroelectric hysteresis loops,[33] the reduction in leakage current, as shown in Fig. 5, may cause the decrease in remnant polarization. However, comparing to the (110) and (111)-oriented thin films, the (001)-oriented BFO thin films have the lowest polarization. As the films' thickness increases, the decreased (001)-orientation should lead to the increase in the films' polarization. However, the improved domain wall motion will increase the polarization of the BFO films due to the reduction of the pinning for the domain wall motion caused by the grain boundary, strain from substrate clamping. As a result, the remnant polarization of the BFO thin films shows weak thickness dependence.

From Fig. 8(f), it is seen that the coercive field decreases with increasing thickness. It is known that the trapped charges in the vicinity of the electrodes are very crucial for the E_c value in the ferroelectric hysteresis loops.[31] The films' surface trapped dentist acted by the microcracks of the thickest BFO films T40 is larger than that of the T20 and T30 as discussed above. Thus, the coercive field of the films T40 should be larger than that of the films T20 or T30, which is

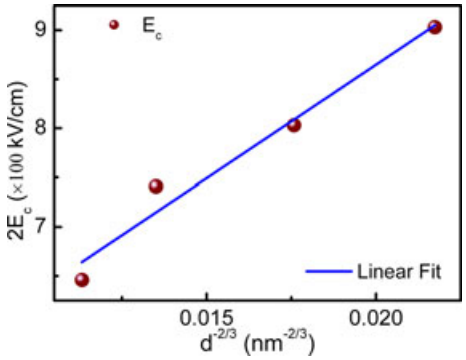

Fig. 9. The variation and fitting of the coercive field versus the thickness with semiempirical scaling law.

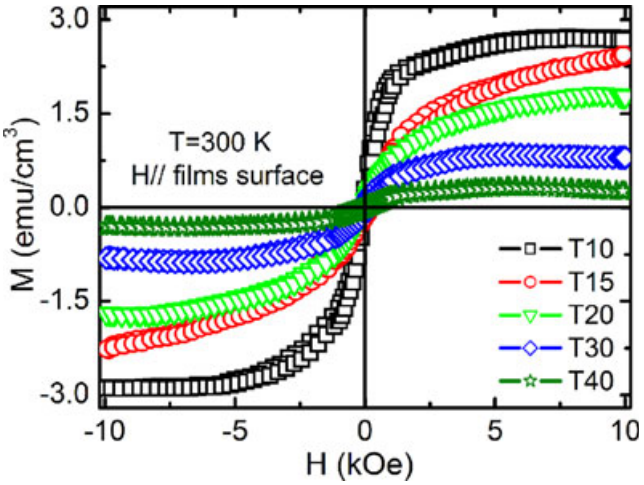

Fig. 10. M–H hysteresis loops of all the films at 300 K.

contrary to the fact. On the other hand, the coercive field due to the existence of the interfacial layer can be described with $E_c = E_{c0} + t_i \cdot f(E_{th})/(d - t_i)$, where E_{C0} is the intrinsic coercive field in the BFO layer, $f(E_{th})$ is a function of the threshold field E_{th} in the interfacial layer.[35] From this equation, it can be concluded that the coercive field decreases with the films' thickness. In addition, the reduction in the pinning of the domain wall motions caused by the grain boundary, strain from substrate clamping, should give some contribution to the decrease in the coercive field of the thick films.[13,19] Thus, the reduction of the coercive field for the thick BFO thin films is attributed to the decrease of the influence interfacial layer, the grain boundary and the strain. Meanwhile, the semiempirical scaling law $E_c(d) \propto d^{-2/3}$ that has been used successfully to describe the thickness dependence of the coercive field in many ferroelectric films,[34] is carried out to fit the results. The fitting result is plotted in the Fig. 9, and shows a well-satisfied scaling law.

(5) Magnetic and Magnetoelectric Properties

Magnetic hysteresis loops of all films measured at 300 K with the magnetic field parallel to the films' surface exhibit weak ferromagnetism as shown in Fig. 10. As the film thickness decreases, the saturated magnetization of the BFO thin films increases. The BFO is a G-type antiferromagnetic structure with a spiral spin modulation wave length of 62 nm.[1,3–5] In addition, the crystallite sizes of all derived films are lower than 62 nm, and incommensurate with the fundamental lattice. It is suggested that the spiral spin structure is suppressed and the uncompensated spins will produce and increase at the crystallite surface with the decreasing crystallite size.[36]

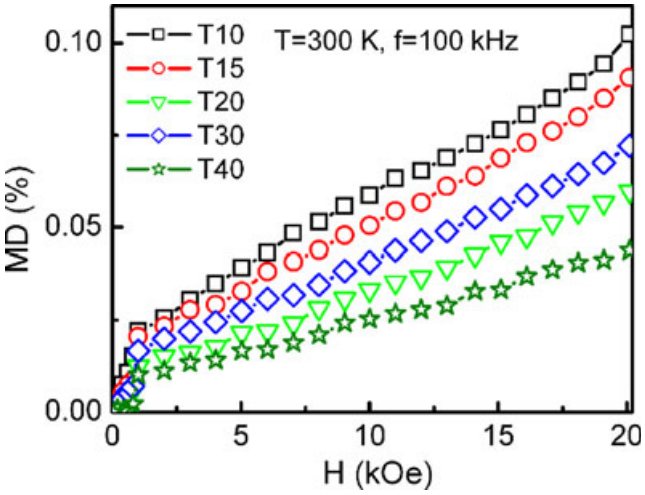

Fig. 11. Magnetic field dependence of dielectric constant measured with 100 kHz at 300 K of all the samples.

The variation of the dielectric constant with applied magnetic field is characterized by the magnetodielectric (MD) parameter defined as $MD\ (\%) = (\varepsilon_H - \varepsilon_{H0})/\varepsilon_{H0} \times 100\%$ where ε_H and ε_{H0} are the dielectric constants with and without applying magnetic field, respectively.[37] The MD method is an alternative way of indirectly characterizing the degree of the magnetoelectric coupling effects.[37] The variation of MD value for all the films versus the applied magnetic fields paralleled the films' surface in the range of 0–20 kOe is plotted in Fig. 11. It is shown that the value of MD increases with the applied magnetic field, and is larger for the thinner films than that of the thicker films. Considering the increased magnetization with decreasing thickness, the increased MD for thinner films can be mainly attributed to the enhanced magnetization. In addition, the contribution of the magnetoresistance effect combined with the Maxwell–Wagner effect cannot be ruled out.[37]

IV. Conclusion

In summary, BFO thin films with different thickness are fabricated by CSD method and the effects of thickness on the microstructure, dielectric, leakage, ferroelectric, magnetic, and magnetoelectric properties are studied. It is observed that, with BFO films' increasing thickness, the crystallization, dielectric, ferroelectric, and leakage properties are improved, whereas the magnetic and magnetoelectric properties are decreased. The leakage is dominated by the space-charges-limited mechanisms. The influences of the interfacial layer on the dielectric constant and leakage current decrease, as the thickness increases. Briefly, to obtain good properties, the optimized thickness of the CSD-derived BFO thin films is within the range of 400–600 nm.

Acknowledgments

This work was supported by the National Science Foundation of China under Contract Nos. 10874051, 50672099, 50802096.

References

[1]J. Wang, J. B. Neaton, H. Zheng, V. Nagarajan, S. B. Ogale, B. Liu, D. Viehland, V. Vaithyanathan, D. G. Schlom, U. V. Waghmare, N. A. Spaldin, K. M. Rabe, M. Wuttig, and R. Ramesh, "Epitaxial $BiFeO_3$ Multiferroic Thin Film Heterostructures," *Science*, **299** [5613] 1719, 4pp (2003).

[2]R. Thomas, J. F. Scott, D. N. Bose, and R. S. Katiyar, "Multiferroic Thin-Film Integration onto Semiconductor Devices," *J. Phys. Condens. Matter*, **22** [42] 3201, 17pp (2010).

[3]Y. E. Roginskaya, Y. N. Venevtsev, S. A. Fedulov, and G. S. Zhdanov, "Nature of Dielectric and Magnetic Properties of $BiFeO_3$," *Sov. Phys. Crystallogr.*, **23** [1] 47, 5pp (1966).

[4]S. V. Kiselev, A. N. Kshnyakina, R. P. Ozerov, and G. S. Zhdanov, "Neutron Diffraction Study of Magnetic Ordering and Atomic Displacements in Some Perovskite Like Substances Containing Iron and Exhibiting Peculiar Dielectric Properties," *Sov. Phys. Solid State*, **5** [11] 2425, 4pp (1964).

[5]F. Kubel and H. Schmid, "Structure of a Ferroelectric and Ferroelastic Monodomain Crystal of the Perovskite $BiFeO_3$," *Acta Crystallogr. Sect. B: Struct. Sci.*, **B46**, 698, 5pp (1990).

[6]R. Y. Zheng, X. S. Gao, Z. H. Zhou, and J. Wang, "Multiferroic $BiFeO_3$ Thin Films Deposited on $SrRuO_3$ Buffer Layer by rf Sputtering," *J. Appl. Phys.*, **101** [5] 054104, 5pp (2007).

[7]M. S. Kartavtseva, O. Y. Gorbenko, A. R. Kaul, A. R. Akbashev, T. V. Murzina, S. Fusil, A. Barthélémy, and F. Pailloux, "$BiFeO_3$ Thin Films Prepared by MOCVD," *Surf. Coat. Technol.*, **201** [22–23] 9149, 5pp (2007).

[8]R. W. Schwartz, "Chemical Solution Deposition of Perovskite Thin Films," *Chem. Mater.*, **9** [11] 2325, 16pp (1997).

[9]S. K. Singh, K. Maruyama, and H. Ishiwara, "Frequency-Dependent Polarization in $BiFeO_3$ Thin Films," *Integrated Ferroelectrics*, **98** [1] 83, 7pp (2008).

[10]H. Naganuma and S. Okamura, "Structural, Magnetic, and Ferroelectric Properties of Multiferroic $BiFeO_3$ Film Fabricated by Chemical Solution Deposition," *J. Appl. Phys.*, **101** [9] 09M103, 3pp (2007).

[11]S. K. Singh, H. Ishiwara, and K. Maruyama, "Enhanced Polarization and Reduced Leakage Current in $BiFeO_3$ Thin Films Fabricated by Chemical Solution Deposition," *J. Appl. Phys.*, **100** [6] 064102, 5pp (2006).

[12]X. W. Tang, J. M. Dai, X. B. Zhu, L. H. Yin, R. Ang, W. H. Song, Z. R. Yang, Y. P. Sun, and R. L. Zhang, "Individual-Layer Thickness Effects on the Preferred c-Axis-Oriented $BiFeO_3$ Films by Chemical Solution Deposition," *J. Am. Ceram. Soc.*, **93** [6] 1682, 6pp (2010).

[13]M. D. Biegalski, D. H. Kim, S. Choudhury, L. Q. Chen, H. M. Christen, and K. Dörr, "Strong Strain Dependence of Ferroelectric Coercivity in a $BiFeO_3$ Film," *Appl. Phys. Lett.*, **98** [14] 142902, 3pp (2011).

[14]F. Tyholdt, H. Fjellvåg, A. E. Gunnæs, and A. Olsen, "Synthesis of Epitaxial $BiFeO_3$ Films by Chemical Solution Deposition on Pt(100)," *J. Appl. Phys.*, **102** [7] 074108, 7pp (2007).

[15]H. S. Chen, J. T. Krause, and E. A. Sigety, "Thermal Expansion and Density of Glassy Pd-Ni-P and Pt-Ni-P Alloys," *J. Non-Cryst. Solids*, **13** [2] 321, 7pp (1974).

[16]J. G. Wu and J. Wang, "Orientation Dependence of Ferroelectric Behavior of $BiFeO_3$ Thin Films," *J. Appl. Phys.*, **106** [10] 104111, 5pp (2009).

[17]C. R. Cho, W. J. Lee, B. G. Yu, and B. W. Kim, "Dielectric and Ferroelectric Response as a Function of Annealing Temperature and the Film Thickness of sol-gel Deposited $Pb(Zr_{0.52},Ti_{0.48})O_3$ Thin Films," *J. Appl. Phys.*, **86** [5] 2700, 12pp (1999).

[18]A. L. Patterson, "The Scherrer Formula for X-Ray Particle Size Determination," *Phys. Rev.*, **56** [10] 978, 5pp (1939).

[19]J. Pérez de la Cruz, E. Joanni, P. M. Vilarinho, and A. L. Kholkin, "Thickness Effect on the Dielectric, Ferroelectric, and Piezoelectric Properties of Ferroelectric Lead Zirconate Titanate Thin Films," *J. Appl. Phys.*, **108** [11] 114106, 8pp (2010).

[20]M. H. Zhao, R. Fu, D. Lu, and T. Y. Zhang, "Critical Thickness for Cracking of $Pb(Zr_{0.53}Ti_{0.47})O_3$ Thin Films Deposited on Pt/Ti/Si(100) Substrates," *Acta Mater.*, **50** [17] 4241, 4pp (2002).

[21]F. Xu, S. T. McKinstry, W. Ren, B. M. Xu, Z. L. Xie, and K. J. Hemker, "Domain Wall Motion and its Contribution to the Dielectric and Piezoelectric Properties of Lead Zirconate Titanate Films," *J. Appl. Phys.*, **89** [2] 1336, 13pp (2001).

[22]M. Dawber, K. M. Rabe, and J. F. Scott, "Physics of Thin-Film Ferroelectric Oxides," *Rev. Mod. Phys.*, **77** [4] 1083, 48pp (2005).

[23]M. A. Lampert and P. Mark, *Current Injection in Solids*. Academic, New York, p. 23, 1970.

[24]C. Wang, M. Takahashi, H. Fujino, X. Zhao, E. Kume, T. Horiuchi, and S. Sakai, "Leakage Current of Multiferroic $(Bi_{0.6}Tb_{0.3}La_{0.1})FeO_3$ Thin Films Grown at Various Oxygen Pressures by Pulsed Laser Deposition and Annealing Effect," *J. Appl. Phys.*, **99** [5] 054104, 5pp (2006).

[25]A. Rose, "Space-Charge-Limited Currents in Single Crystal of Cadmium Sulfide," *Phys. Rev.*, **97** [6] 1538, 6pp (1955).

[26]X. Qi, J. Dho, R. Tomov, M. G. Blamire, and J. L. M. Driscoll, "High-Resolution X-ray Diffraction and Transmission Electron Microscopy of Multiferroic $BiFeO_3$ Films," *Appl. Phys. Lett.*, **86** [7] 062903, 3pp (2005).

[27]J. F. Scott, C. A. Araujo, B. M. MElnick, L. D. McMillan, and R. Zuleeg, "Quantitative Measurement of Space-Charge Effects in Lead Zirconate-Titanate Memories," *J. Appl. Phys.*, **70** [1] 382, 7pp (1991).

[28]P. K. Larsen, G. J. Dormas, D. J. Taylor, and P. I. van Veldhoven, "Thickness Effect on the Dielectric, Ferroelectric, and Piezoelectric Properties of Ferroelectric Lead Zirconate Titanate Thin Films," *J. Appl. Phys.*, **76** [4] 2405, 8pp (1994).

[29]J. Z. Huang, Y. Wang, Y. H. Lin, M. Li, and C. W. Nan, "Effect of Mn Doping on Electric and Magnetic Properties of $BiFeO_3$ Thin Films by Chemical Solution Deposition," *J. Appl. Phys.*, **106** [6] 063911, 5pp (2009).

[30]S. K. Singh, R. Ueno, H. Funakubo, H. Uchida, S. Koda, and H. Ishiwara, "Dependence of Ferroelectric Properties on Thickness of $BiFeO_3$ Thin Films Fabricated by Chemical Solution Deposition," *Jpn. J. Appl. Phys.*, **44** [12] 8525, 3pp (2005).

[31]J. F. M. Cillessen, M. W. J. Prins, and R. M. Wolf, "Thickness Dependence of the Switching Voltage in All-Oxide Ferroelectric Thin-Film Capacitors Prepared by Pulsed Laser Deposition," *J. Appl. Phys.*, **81** [6] 2777, 7pp (1997).

[32]S. M. Sze, *Physics of Semiconductor Devices*, 2nd edition. Wiley, New York, 1981.

[33]A. Z. Simões, A. H. M. Gonzalez, L. S. Cavalcante, C. S. Riccardi, E. Longo, and J. A. Varela, "Ferroelectric Characteristics of $BiFeO_3$ Thin Films Prepared via a Simple Chemical Solution Deposition," *J. Appl. Phys.*, **101** [7] 074108, 6pp (2007).

[34]J. F. Scott, "Comment on "Quantum Confinement Effects on the Optical and Dielectric Properties for Mesocrystals of $BaTiO_3$ and $SrBi_2Ta_2O_9$," *J. Appl. Phys.*, **88** [10] 6092, 1pp (2000).

[35]A. K. Tagantsev and I. A. Stolichnov, "Injection-Controlled Size Effect on Switching of Ferroelectric Thin Films," *Appl. Phys. Lett.*, **74** [9] 1326, 3pp (1999).

[36]T. J. Park, G. C. Papaefthymiou, A. J. Viescas, A. R. Moodenbaugh, and S. S. Wong, "Size-Dependent Magnetic Properties of Single-Crystalline Multiferroic $BiFeO_3$ Nanoparticles," *Nano Lett.*, **7** [3] 766, 7pp (2007).

[37]G. Catalan, "Magnetocapacitance without Magnetoelectric Coupling," *Appl. Phys. Lett.*, **88** [10] 102902, 3pp (2006). □